8994 *Biochemistry* **2009,** *48,* 8994–9001
DOI: 10.1021/bi901195e

BIOCHEMISTRY
including biophysical chemistry & molecular biology
Article

Structural Coupling of a Tyrosine Side Chain with the Non-Heme Iron Center in Photosystem II As Revealed by Light-Induced Fourier Transform Infrared Difference Spectroscopy[†]

Ryouta Takahashi,[‡] Alain Boussac,[§] Miwa Sugiura,[∥] and Takumi Noguchi*[,‡]

[‡]*Institute of Materials Science, University of Tsukuba, Tsukuba, Ibaraki 305-8573, Japan,* [§]*iBiTec-S, SB2SM, URA CNRS 2096, CEA Saclay, 91191 Gif sur Yvette, France, and* [∥]*Cell-Free Science and Technology Research Center, Ehime University, Matsuyama, Ehime 790-8577, Japan*

Received July 14, 2009; Revised Manuscript Received August 20, 2009

ABSTRACT: The non-heme iron is located between the quinone electron acceptors, Q_A and Q_B, in photosystem II (PSII), and together with its bicarbonate ligand, it regulates the electron and proton transfer reactions of quinone acceptors. In this study, we have investigated the structural coupling of a nearby Tyr residue with the non-heme iron center using Fourier transform infrared (FTIR) spectroscopy. Light-induced Fe^{2+}/Fe^{3+} FTIR difference spectra of PSII core complexes from unlabeled and [4-^{13}C]Tyr-labeled *Thermosynechococcus elongatus* revealed that the CO stretching (νCO) bands of a Tyr side chain are located at 1253 and 1241 cm^{-1} in the Fe^{2+} and Fe^{3+} states, respectively. Upon deuteration, both νCO bands were upshifted by 11−12 cm^{-1}. Taking into account the criteria for determining the hydrogen bond structure of a Tyr side chain from infrared bands reported previously [Takahashi, R., and Noguchi, T. (2007) *J. Phys. Chem. B 111*, 13833−13844] and the results of DFT calculations of model complexes of *p*-cresol hydrogen-bonded with bicarbonate, we interpreted the observed νCO bands and their deuteration effects as indicating that one Tyr side chain with a hydrogen bond donor−acceptor form is strongly coupled to the non-heme iron. From the X-ray structures of PSII core complexes, it is proposed that either D1-Y246 or D2-Y244 provides a hydrogen bond to the oxygen of the bicarbonate ligand but the other Tyr does not directly interact with bicarbonate. The Tyr residue coupled to the non-heme iron may play a key role in the regulatory function of the iron−bicarbonate center by stabilizing the bicarbonate ligand and forming a rigid hydrogen bond network around the non-heme ion.

Photosystem II (PSII)[1] is a multimeric protein complex that functions as a water-quinone oxidoreductase. Light illumination to PSII triggers charge separation between the special pair chlorophyll P680 and the pheophytin electron acceptor. On the electron donor side, $P680^+$ oxidizes the Mn cluster through Y_Z and two water molecules are converted to a molecular oxygen and four protons (*1*), while on the electron acceptor side, an electron is transferred from the pheophytin to the primary quinone electron acceptor Q_A and then to the secondary quinone acceptor Q_B (*2*). When Q_B is doubly reduced, it is protonated and released from the protein pocket as a quinol molecule.

The non-heme iron is located between Q_A and Q_B (*2*−*4*). As revealed by the X-ray crystallographic structures of PSII core complexes (*5*−*7*), the non-heme iron is ligated by four His residues, D1-His215, D1-His272, D2-His214, and D1-His268, and a bicarbonate ion (Figure 1). D2-His214 and D1-His215 bridge the non-heme iron with Q_A and Q_B, respectively, through hydrogen bonding interactions. Such a structure around the non-heme iron is virtually identical to that of a bacterial type II reaction center, which is thought to be the prototype of PSII in its evolution, except that the bacterial non-heme iron has a Glu ligand instead of bicarbonate (*8*). The Fe^{2+}/Fe^{3+} redox couple of the non-heme iron in PSII has a midpoint potential (E_m) of 400 mV at pH 7 (*9*, *10*), which is much lower than the bacterial one ($E_m \geq 550$ mV) (*4*). Hence, the iron center in PSII is readily oxidized to Fe^{3+} by ferricyanide, and then it can be photoreduced to Fe^{2+} by accepting an electron from Q_A^-. The pH dependence of E_m with −60 mV/pH (*10*, *11*) implies that this redox reaction is coupled to proton transfer, suggesting the presence of a proton pathway in a hydrogen bond network around the non-heme iron center (*12*). Indeed, proton uptake upon photoreduction of Fe^{3+} has been detected (*13*−*15*). A recent theoretical work also revealed the existence of a network of residues serving as an internal proton reservoir around the iron center (*16*).

The bicarbonate ligand, which was introduced to PSII in the evolutionary process via replacement of the Glu ligand in bacterial reaction centers, must have some specific function. The bicarbonate is a labile ligand and is readily replaced with NO, CN^-, and many carboxylate anions (*2*−*4*). Thus, bicarbonate has been

[†]This study was supported by the JSPS and CNRS under the Japan-France Research Cooperative Program, Grants-in-Aid for Scientific Research from the Ministry of Education, Culture, Sports, Science and Technology to T.N. (17GS0314, 21108506, and 21370063), and a Grant-in-Aid for JSPS fellows (204647) to R.T.

*To whom correspondence should be addressed. Phone: +81-29-853-5126. Fax: +81-29-853-4490. E-mail: tnoguchi@ims.tsukuba.ac.jp.

[1]Abbreviations: νCO, CO stretching vibration; δCOH, COH bending vibration; DFT, density functional theory; DM, *n*-dodecyl β-D-maltoside; FTIR, Fourier transform infrared; IR, infrared; PSII, photosystem II; P680, special pair chlorophyll of photosystem II; Q_A, primary quinone electron acceptor; Q_B, secondary quinone electron acceptor; Y_D, redox-active tyrosine on the D2 protein; Y_Z, redox-active tyrosine on the D1 protein.

 Published on Web 08/21/2009

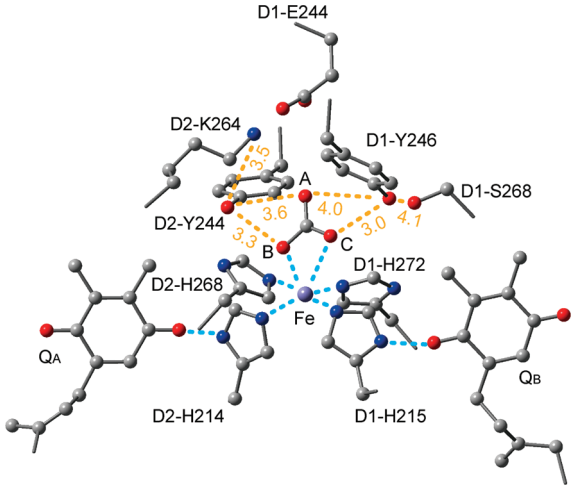

FIGURE 1: X-ray structure around the non-heme iron of the PSII complex from *Thermosynechococcus elongatus* (*7*). The distances (angstroms) from D1-Y246 and D2-Y244 to the bicarbonate and nearby residues are also presented (orange). The oxygen atoms of the bicarbonate are designated as O_A, O_B, and O_C.

proposed to play regulatory roles in the acceptor side reactions (*2*−*4*, *17*−*19*). It is essential for proper electron flow from Q_A to Q_B, and the electron transfer rate is slowed by bicarbonate depletion (*2*, *4*, *20*). Bicarbonate is also necessary for protonation of Q_B^{2-} and hence is proposed to be involved in the proton pathway to Q_B (*4*, *14*, *17*, *21*). The exchange of bicarbonate with other carboxylate anions alters the E_m of the non-heme iron and its pH dependence (*22*), suggesting that bicarbonate regulates the pK_a of protonatable groups near the iron center through hydrogen bond networks.

The X-ray structures of PSII core complexes showed that two Tyr residues, D1-Y246 and D2-Y244, are located in the vicinity of the non-heme iron and within hydrogen bonding distance of the bicarbonate (Figure 1). D2-K264, D1-E244, and D1-S268 also exist around the bicarbonate and seem to form a hydrogen bond network together with the Tyr side chains. However, the limited resolution of the X-ray structures (2.9−3.5 Å) (*5*−*7*) and inherent difficulty in detecting protons by X-ray crystallography have hampered clarification of the hydrogen bonding structures around the iron−bicarbonate center, which is essential for understanding the molecular mechanism of bicarbonate regulation of quinone reactions.

In this study, we have investigated the hydrogen bond interactions of the iron−bicarbonate center focusing on the nearby Tyr residues. To do so, we used light-induced Fourier transform infrared (FTIR) difference spectroscopy, which is especially sensitive to protonation and hydrogen bond structures of amino acid side groups and has been used in investigation of the structures and reactions of PSII (*23*−*27*). FTIR spectra specific to the non-heme iron center have been obtained as Fe^{2+}/Fe^{3+} difference spectra by utilizing photoreduction of Fe^{3+} and revealed the bicarbonate and histidine ligation, the pH-dependent redox potential, and the coupling with proton transfer reactions (*14*, *28*−*30*). Tyr signals coupled to cofactor reactions can be identified in FTIR difference spectra using selective isotope labeling of Tyr side chains (*31*−*34*). We have further performed DFT calculations using model complexes of *p*-cresol hydrogen-bonded with bicarbonate to determine the hydrogen bond structure of Tyr coupled to the non-heme iron. The obtained results revealed that one Tyr side chain is strongly coupled to the non-heme iron though a hydrogen bond to bicarbonate.

MATERIALS AND METHODS

PSII core complexes of *T. elongatus*, in which the carboxyl terminus of the CP43 subunit was genetically His-tagged, were purified as previously described (*35*). [4-^{13}C]Tyr labeling of *T. elongatus* cells was performed as described in ref *36* using L-[4-^{13}C]Tyr. Mn depletion was performed with 10 mM NH_2OH treatment for 30 min at room temperature (*35*).

The Mn-depleted PSII core complexes were suspended in a pH 8.0 Tris buffer in the presence of bicarbonate (10 mM Tris, 20 mM sucrose, 5 mM NaCl, 10 mM $NaHCO_3$, and 0.06% DM) and concentrated to 9 mg of chlorophyll/mL using a Microcon-100 apparatus (Amicon). For Fe^{2+}/Fe^{3+} FTIR measurements, an aliquot (5 μL) of the sample suspension was mixed with 1 μL of 500 mM potassium ferricyanide and deposited on a ZnSe plate (25 mm in diameter). The sample was then lightly dried under a N_2 gas flow and sandwiched with another ZnSe plate together with 1 μL of H_2O (or D_2O) (*37*). One of the ZnSe plates has a circular groove (14 mm inner diameter, 1 mm width), and the sample cell was sealed with silicone grease laid on the outer part of the groove, where a piece of aluminum foil (~1 mm × 1 mm, ~15 μm thick) was placed as a spacer. Deuterated PSII core complexes were prepared by resuspending a dried sample on the ZnSe plate with a small volume of D_2O (Aldrich, 99.9 at. % D). The sample temperature was adjusted to 10 °C by circulating cold water in a copper holder. The sample was stabilized at this temperature in the dark for more than 1 h before measurements were started.

Flash-induced FTIR spectra were recorded on a Bruker IFS-66/S spectrophotometer equipped with an MCT detector (D313-L) at 4 cm^{-1} resolution. Flash illumination was performed using a Q-switched Nd:YAG laser (INDI-40-10, 532 nm, ~7 ns full width at half-maximum, 10 mJ $pulse^{-1}$ cm^{-2}). Single-beam spectra with 50 scans (25 s accumulation) were recorded before and after single-flash illumination. The measurement was repeated with an interval of 300 s for dark relaxation. The spectra obtained by more than 220 cycles using one or two samples were averaged to calculate a Fe^{2+}/Fe^{3+} difference spectrum by subtracting the spectrum before illumination from that after illumination.

Spectral fitting was performed using IGOR Pro (WaveMetrics Inc., Lake Oswego, OR).

Molecular orbital calculations were performed using the Gaussian03 program package (*38*). The B3LYP functional (*39*, *40*) with the 6-31+G(d,p) basis set was used to optimize the geometries of model complexes and calculate their vibrational frequencies and IR intensities. The calculated frequencies were scaled with a scaling factor of 0.977 following the previous report (*41*).

RESULTS

Fe^{2+}/Fe^{3+} FTIR Difference Spectra. Figure 2a (black line) shows a Fe^{2+}/Fe^{3+} FTIR difference spectrum of Mn-depleted PSII core complexes from *T. elongatus* in a pH 8 buffer. The positive and negative signals reflect the structures in the Fe^{2+} and Fe^{3+} states, respectively. The peaks at 2115(+)/2040(−) cm^{-1} arising from the CN stretches of ferricyanide/ferrocyanide (data not shown) indicate that an electron is donated from ferrocyanide on the electron donor side. The observed spectral features were

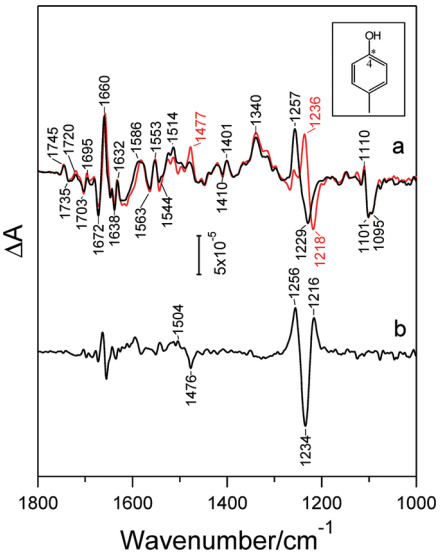

FIGURE 2: (a) Light-induced Fe^{2+}/Fe^{3+} FTIR difference spectra obtained using unlabeled (black line) and [4-^{13}C]Tyr-labeled (red line) PSII core complexes at pH 8.0. The inset shows the structure of a Tyr side chain, in which the carbon atom labeled with ^{13}C is marked with an asterisk. (b) Double-difference spectrum between the [4-^{13}C]-Tyr-labeled and unlabeled spectra (unlabeled minus [4-^{13}C]Tyr-labeled).

basically identical to those of the previous Fe^{2+}/Fe^{3+} FTIR difference spectra obtained using spinach PSII membranes (*14*, *28*, *29*) and the core complexes of *T. elongatus* (*30*). The complex structures in the 1700−1600 and 1600−1500 cm^{-1} region include the amide I and amide II bands, respectively, originating from conformational changes of polypeptide main chains. Hienerwadel and Berthomieu (*28*) assigned the bands at 1340(+) and 1229(−) cm^{-1} to the symmetric νCO vibrations of the bicarbonate ligand in the Fe^{2+} and Fe^{3+} states, respectively, by replacing bicarbonate with [^{13}C]bicarbonate. This isotope labeling analysis also revealed that the coupled asymmetric νCO vibrations of bicarbonate are present at 1530 and 1658 cm^{-1} in the Fe^{2+} and Fe^{3+} states, respectively, and the presence of the bicarbonate δCOH mode at 1258 cm^{-1} in the Fe^{2+} state. Global ^{15}N labeling of PSII membranes showed that the positive peak at 1110 cm^{-1} and the negative peaks at 1101 and 1095 cm^{-1} arise from the νCN vibrations of His ligands (*28*). The νC=O bands of the COOH groups of carboxylic amino acids and of the ester groups of chlorophyll or pheophytin may be involved in the 1750−1700 cm^{-1} region. Contributions of Arg and Lys signals to the 1680−1500 cm^{-1} region, of carboxylate side chains to the 1563/1586 and 1410/1401 cm^{-1} bands (1561/1585 and 1409/1400 cm^{-1} in ref *28*), and of the Tyr νCO signal to the 1257 cm^{-1} band were also suggested.

If a Tyr side chain is structurally coupled to the non-heme iron through hydrogen bond interactions, νCO and δCOH bands of the COH group of Tyr should appear in the region of 1300−1150 cm^{-1} (*41*, *42*). To identify Tyr bands in the Fe^{2+}/Fe^{3+} difference spectrum, we replaced Tyr side chains in the PSII core complexes with [4-^{13}C]Tyr, in which the carbon atom having an OH group is labeled with ^{13}C (Figure 2, inset). The obtained spectrum of the [4-^{13}C]Tyr-labeled PSII complexes is presented in Figure 2a (red line). The spectrum was scaled so that the intensity of the ferricyanide peak at 2115 cm^{-1} matched that of the unlabeled sample (not shown). Significant spectral changes were observed at 1300−1200 cm^{-1} in the Tyr νCO and δCOH region. The positive and negative peaks at 1257 and 1229 cm^{-1} showed clear

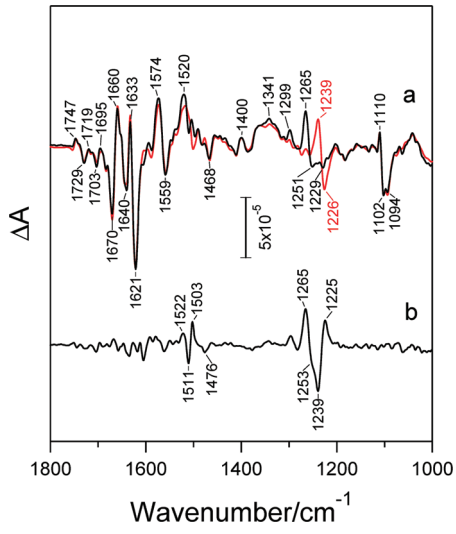

FIGURE 3: (a) Light-induced Fe^{2+}/Fe^{3+} FTIR difference spectra obtained using unlabeled (black line) and [4-^{13}C]Tyr-labeled (red line) PSII core complexes in D_2O. (b) Double-difference spectrum between the [4-^{13}C]Tyr-labeled and unlabeled spectra in D_2O (unlabeled minus [4-^{13}C]Tyr-labeled).

downshifts to 1236 and 1218 cm^{-1} by 21 and 11 cm^{-1}, respectively.

For more detailed analysis, we extracted only Tyr bands from the Fe^{2+}/Fe^{3+} spectrum by calculating a double-difference spectrum between the [4-^{13}C]Tyr-labeled and unlabeled spectra (unlabeled minus [4-^{13}C]Tyr-labeled) (Figure 2b). Prominent bands were observed at 1256(+), 1234(−), and 1217(+) cm^{-1}, whereas other bands were mostly canceled. Small signals at ~1504 and 1476 cm^{-1} are probably due to $Y_D^{\bullet}$ that contaminates the Fe^{2+}/Fe^{3+} spectrum. In fact, previous studies reported the νCO peaks of unlabeled and [4-^{13}C]Tyr-labeled $Y_D^{\bullet}$ at 1503 and 1477 cm^{-1}, respectively (*31*−*33*). The νCO/δCOH bands of Y_D in the 1290−1200 cm^{-1} region, however, exhibited much smaller intensities (by ~0.3) than the νCO intensity of $Y_D^{\bullet}$ at pH > 8 (*32*), which was used in this study. Thus, the contribution of the Y_D signals to the bands in the 1260−1210 cm^{-1} region is negligible. The peaks in the amide I region (~1650 cm^{-1}) are not reproducible and are probably ascribed to a subtle difference in the sample conditions, to which amide I bands are generally very sensitive.

Similar measurements were performed for samples in D_2O. In deuterated Tyr, the δCOD vibration occurs at a frequency lower than 1000 cm^{-1}, and hence, the δCOH vibrations disappear from the 1300−1200 cm^{-1} region leaving only νCO bands (*34*, *41*). The Fe^{2+}/Fe^{3+} difference spectrum of unlabeled PSII core complexes in D_2O is shown in Figure 3a (black line). The effects of deuteration are similar to those in spinach PSII membranes previously reported by Hienerwadel and Berthomieu (*28*). The relative intensity of the 1229 cm^{-1} peak decreased, and the 1257 cm^{-1} peak in H_2O upshifted to 1265 cm^{-1}, making a negative intensity at 1251 cm^{-1} apparent. In the amide I region, new strong peaks appeared at 1633(+) and 1621(−) cm^{-1}. These changes indicate that protonatable groups around the non-heme iron were successfully deuterated by incubation of the core sample in D_2O for a relatively short period of time (~1 h before measurement).

The [4-^{13}C]Tyr-labeled PSII sample in D_2O exhibited peaks at 1239(+) and 1226(−) cm^{-1} (Figure 3a, red line) as a result of downshifts by 26 and 25 cm^{-1} of the 1265(+) and 1251(−) cm^{-1}

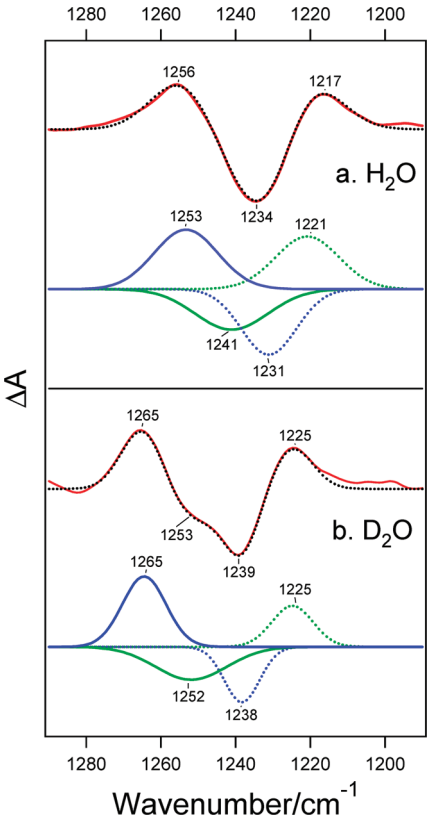

FIGURE 4: νCO/δCOH region of Tyr in the isotope-edited double-difference spectra (unlabeled minus [4-^{13}C]Tyr-labeled) (red lines) in H_2O (A) and D_2O (B) and deconvolution of the spectra into Gaussian bands (blue and green lines). In the latter Gaussian bands, blue and green lines represent the bands in the Fe^{2+} and Fe^{3+} states, respectively, and solid and dotted lines represent the bands of unlabeled and 4-^{13}C-labeled Tyr, respectively. The sum of the Gaussian bands (black dotted line) is overlaid on the experimental spectrum.

peaks, respectively, of unlabeled PSII in D_2O. In the unlabeled minus [4-^{13}C]Tyr-labeled double-difference spectrum (Figure 3b), these changes are revealed as peaks at 1265(+), 1253(−), 1239(−), and 1225(+) cm^{-1}. A minor differential signal around 1290 cm^{-1} on the higher-frequency side of these signals probably originates from the ring νCC and δCH mode weakly coupled with the δCOD vibration according to our DFT calculation of *p*-cresol, in which this mode downshifts by ~10 cm^{-1} upon 4-^{13}C labeling whereas the corresponding mode in nondeuterated *p*-cresol is unaffected. A small negative band at 1476 cm^{-1} and some contribution to the 1503 cm^{-1} band are probably due to the νCO signal of contaminating $Y_D^{\bullet}$, in analogy with the corresponding signals in H_2O, while peaks at 1522(+), 1511(−), and 1503(+) cm^{-1} may be mainly attributed to the 19a mode of Tyr arising from the νCC and δCH vibrations (*41*). Previous studies of Y_D in PSII (*31*−*33*) and the photocycle of the cyanobacterial sensor protein TePixD (*34*) have shown the 19a bands in similar positions in corresponding double-difference spectra. The reason why the 19a bands did not clearly appear in the spectrum in H_2O (Figure 2b) is unknown but could be due to some coincidental overlap of bands.

To further characterize the νCO/δCOH bands of Tyr, the obtained double-difference spectra in the 1280−1200 cm^{-1} region were decomposed into Gaussian bands by a fitting procedure (Figure 4). Frequencies, intensities, and widths of Gaussian bands were changed as parameters without any constraints in the fitting. Not only the double-difference spectrum in D_2O (Figure 4b) but also that in H_2O (Figures 4a) was successfully

Table 1: Frequencies (cm^{-1}) of the νCO Bands of the Tyr Coupled to the Non-Heme Iron in the Fe^{3+} and Fe^{2+} States Obtained by Fitting Analysis of the Unlabeled minus [4-^{13}C]Tyr-Labeled Double-Difference Spectra

	Fe^{2+}			Fe^{3+}		
	[^{12}C]Tyr	[4-^{13}C]Tyr	Δ^{13}C[a]	[^{12}C]Tyr	[4-^{13}C]Tyr	Δ^{13}C[a]
in H_2O	1253	1231	−22	1241	1221	−20
in D_2O	1265 (+12)[b]	1238	−27	1252 (+11)[b]	1225	−27

[a]Frequency shifts upon [4-^{13}C]Tyr labeling. [b]Values in parentheses are frequency shifts upon deuteration.

reproduced by the sum of four Gaussian bands. This is a sharp contrast to the similar analysis of Tyr νCO/δCOH bands of TePixD, in which eight bands were necessary to fit the double-difference spectrum in H_2O (*34*). The obtained frequencies of the Gaussian bands are summarized in Table 1. In the Fe^{2+} and Fe^{3+} states, the bands are found at 1253 and 1241 cm^{-1}, respectively, which upshift by 11−12 cm^{-1} to 1265 and 1252 cm^{-1}, respectively, upon deuteration. The bands of unlabeled samples downshift by 20−27 cm^{-1} upon [4-^{13}C]Tyr labeling both in H_2O and in D_2O. It is noted that similar analysis after removal of the contribution of $Y_D^{\bullet}/Y_D$ contamination from the spectra provided basically the same result except for slight shifts of some peaks by less than 3 cm^{-1}.

DFT Calculations for Model Complexes of p-Cresol Hydrogen-Bonded with Bicarbonate. Frequencies and IR intensities of the νCO and δCOH vibrations of model complexes of *p*-cresol, a simplest model of a Tyr side chain, hydrogen-bonded with a bicarbonate anion were calculated using the DFT method at the B3LYP/6-31+G(d,p) level. In model 1, *p*-cresol has a hydrogen bond donor form and is hydrogen-bonded only with bicarbonate, whereas in models 2 and 3, *p*-cresol forms two hydrogen bonds with bicarbonate and methanol as a hydrogen bond donor−acceptor form (Figure 5). In the latter two models, *p*-cresol provides a hydrogen bond to the oxygen atom of the bicarbonate OH (model 2) or CO (model 3) group. The optimized geometries of these complexes are depicted in Figure 5, and the calculated frequencies and IR intensities are summarized in Table 2. It is shown that hydrogen bond distances between *p*-cresol and bicarbonate [1.708, 1.642, and 1.466 Å in models 1−3, respectively (Figure 5)] are shorter than those in any of the model complexes of *p*-cresol hydrogen-bonded with various neutral compounds in ref *41*, reflecting strong hydrogen bonds with anionic bicarbonate. Model 1 provides the νCO and δCOH vibrations at 1285 and 1264 cm^{-1}, respectively, with comparable strong IR intensities. In sharp contrast, models 2 and 3 provide a strong νCO vibration and an almost IR-inactive δCOH vibration. The νCO frequency of 1296 cm^{-1} in model 3 is much higher than that of 1266 cm^{-1} in model 2, indicating that the νCO frequency significantly increases when *p*-cresol is hydrogen-bonded to a negatively charged oxygen atom. Upon deuteration of the *p*-cresol OH group, the νCO frequency of model 1 downshifts by 8 cm^{-1}, whereas models 2 and 3 exhibit smaller downshifts of 1 and 4 cm^{-1}, respectively. The effect of 4-^{13}C labeling is similar in all three models; the νCO frequency downshifts by 22−23 cm^{-1}, while smaller downshifts of 16−19 cm^{-1} are seen in the δCOH frequency (Table 2).

DISCUSSION

Structural Coupling of Tyr with the Non-Heme Iron. Selective labeling of Tyr side chains with [4-^{13}C]Tyr in the PSII

core complexes from *T. elongatus* clearly revealed the presence of Tyr signals in the Fe^{2+}/Fe^{3+} FTIR spectrum (Figure 2). The prominent bands at 1257(+) and 1229(−) cm^{-1} exhibited significant downshifts to 1236 and 1218 cm^{-1}, respectively. Hienerwadel and Berthomieu (*28*) previously proposed a tentative assignment of the 1257 cm^{-1} peak to the νCO vibration of Tyr superimposing the δCOH band of bicarbonate. Our study provides definitive proof of this assignment of the Tyr peak in the Fe^{2+} state. We also showed that the Tyr signal in the Fe^{3+} state gives some contribution to the negative band at 1229 cm^{-1}, which mainly arises from the symmetric νCO vibration of bicarbonate. The presence of Tyr signals in the Fe^{2+}/Fe^{3+} spectrum indicates that a Tyr side chain(s) is structurally coupled to the non-heme iron center and affected by the Fe^{2+}/Fe^{3+} redox change.

The bands of Tyr were extracted from the Fe^{2+}/Fe^{3+} spectrum by calculation of a double-difference spectrum between the spectra of [4-^{13}C]Tyr-labeled and unlabeled PSII (Figures 2b and 3b). In both H_2O and D_2O, the double-difference spectrum in the 1280−1200 cm^{-1} region, in which the νCO and δCOH vibrations of Tyr are located (*31*−*34*, *41*, *42*), was successfully reproduced by the sum of four Gaussian bands, two of which are attributed to [^{12}C]Tyr in the Fe^{2+} and Fe^{3+} states and the other two of which are the corresponding bands of [4-^{13}C]Tyr (Figure 4). Thus, the bands of [^{12}C]Tyr were identified at 1253 and 1241 cm^{-1} in the Fe^{2+} and Fe^{3+} states, respectively, while upon deuteration of the OH group, the bands were found at 1265 and 1252 cm^{-1} as a result of upshifts by 12 and 11 cm^{-1}, respectively (Table 1). The significant deuteration effect together with the frequencies lower than ~1270 cm^{-1} typical of the νCO frequency of the tyrosinate form (*31*, *33*) indicates that the Tyr coupled with the non-heme iron takes a protonated form in both the Fe^{2+} and Fe^{3+} states.

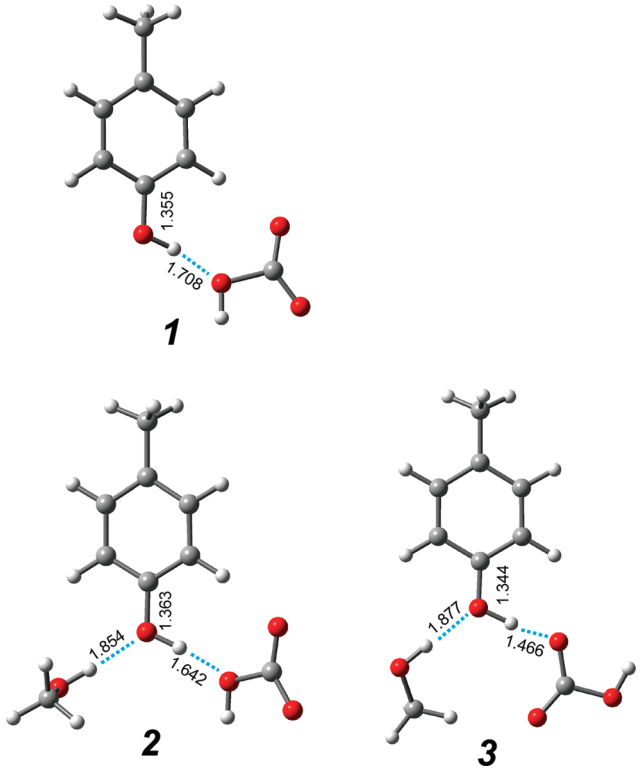

FIGURE 5: Optimized geometries of model complexes of *p*-cresol hydrogen-bonded with bicarbonate. In model 1, *p*-cresol is hydrogen-bonded with the oxygen atom of the bicarbonate OH group. In model 2, *p*-cresol is hydrogen-bonded with the oxygen atom of the bicarbonate OH group and the hydrogen atom of the methanol OH group. In model 3, *p*-cresol is hydrogen-bonded with the oxygen atom of the bicarbonate CO group and the hydrogen atom of the methanol OH group.

Hydrogen Bond Structure of the Tyr Side Chain. Takahashi and Noguchi (*41*) recently proposed criteria for determining the hydrogen bond structures of a Tyr side chain using its νCO and δCOH IR bands from the results of DFT calculations of various hydrogen-bonded complexes of *p*-cresol together with experimental observations of Tyr and *p*-cresol. It was reported that νCO vibrations occur at 1280−1260, 1260−1250, 1255−1235, and 1240−1220 cm^{-1} in the hydrogen bond donor, free, donor−acceptor, and acceptor forms, respectively, while δCOH vibrations are found at 1255−1210 cm^{-1} in the donor form and at relatively low frequencies of 1190−1160 cm^{-1} in the free and acceptor forms. The notable result was that in the donor−acceptor form, the δCOH vibration located at 1260−1240 cm^{-1} was almost IR-inactive (*41*). Another characteristic of the donor−acceptor form is that deuteration of the OH group provides a similar or even upshifted (sometimes by more than 10 cm^{-1}) νCO frequency, whereas other forms always exhibit downshifts of the νCO frequencies by several wavenumbers (*41*).

These criteria were, however, determined for Tyr and *p*-cresol complexes hydrogen-bonded with neutral compounds. Since it was uncertain that the same criteria can be used to analyze the bands of Tyr hydrogen-bonded to an anion like bicarbonate, we have performed DFT calculations for model complexes of *p*-cresol hydrogen-bonded with bicarbonate (Figure 5 and Table 2). Although both of the νCO and δCOH vibrations exhibited frequencies higher than the frequency range for complexes with neutral hydrogen bond partners due to stronger hydrogen bonding, the basic characteristics of the νCO and δCOH vibrations dependent on the hydrogen bond forms were conserved. First, in the donor−acceptor form (models 2 and 3), the δCOH mode was almost IR-inactive, whereas in the donor form (model 1), the δCOH exhibited an intensity comparable to that of the νCO vibration (Table 2). Second, the downshift of the νCO frequency by deuteration is smaller (1−4 cm^{-1}) in the donor−acceptor

Table 2: Calculated Frequencies (cm^{-1}) and IR Intensities (km mol^{-1}) of the νCO and δCOH Vibrations of *p*-Cresol in Its Hydrogen-Bonded Complexes with Bicarbonate

	νCO[b]			δCOH[b]	
hydrogen bond partner (complex no.)[a]	frequency (intensity)[c]	ΔD[d]	Δ4-^{13}C[e]	frequency (intensity)[c]	Δ4-^{13}C[e]
bicarbonate O(H) (1)	1285 (87)	−8	−22	1264 (117)	−16
bicarbonate O(H)/methanol (2)	1266 (219)	−1	−23	1283 (2)	−18
bicarbonate CO/methanol (3)	1296 (199)	−4	−22	1279 (6)	−19

[a]The complex number and the optimized geometries are presented in Figure 5. [b]Calculated frequencies (cm^{-1}) were scaled by a factor of 0.977 following ref *41*. [c]Values in parentheses are IR intensities (km mol^{-1}). [d]Shifts upon deuteration of the OH group of *p*-cresol. [e]Shifts upon 4-^{13}C labeling.

form than that in the donor form (8 cm^{-1}). Thus, although the νCO frequency was not upshifted by deuteration in models 2 and 3 used in this study, a general tendency of the deuteration effect on the νCO vibration seems to hold even in the case of Tyr−bicarbonate complexes.

By application of the criteria described above to the Tyr bands coupled to the non-heme iron, the free and acceptor forms are readily excluded from candidates, because no δCOH bands were observed in the low-frequency region of 1190−1160 cm^{-1} in the double-difference spectrum of Fe^{2+}/Fe^{3+} in H_2O (Figure 2b). The observation that only a single band of Tyr was found for each of the Fe^{2+} and Fe^{3+} states [at 1253 and 1241 cm^{-1}, respectively (Table 1)] is consistent with the band pattern of the donor−acceptor form, in which only the νCO band is strong and the δCOH band is almost IR-inactive. The assignments of the 1253 and 1241 cm^{-1} bands to the νCO vibrations are also supported by the downshifts of 20−22 cm^{-1} upon 4-^{13}C labeling (Table 1), which is consistent with the calculated result in Table 2 and in the previous study (Supporting Information of ref *41*). The δCOH vibrations usually exhibit 4-^{13}C-induced downshifts of <20 cm^{-1} (Table 2 and ref *41*). In addition, the νCO bands upshifted by 12 and 11 cm^{-1} upon deuteration (Table 1), which is inconsistent with the tendency of the νCO downshift upon deuteration in the donor form but consistent with the often observed upshift in the donor−acceptor form (*41*). The νCO frequencies at 1253/1241 cm^{-1} in H_2O and 1265/1252 cm^{-1} in D_2O in the Fe^{2+}/Fe^{3+} states are within or slightly higher than the typical νCO range of the donor−acceptor form [1255−1235 cm^{-1} in H_2O and 1260−1240 cm^{-1} in D_2O (*41*)]. The relatively high νCO frequencies are consistent with a hydrogen bond interaction with a bicarbonate anion, although the anionic nature should be significantly reduced by ligation to Fe^{2+} or Fe^{3+} compared with free bicarbonate in the model complexes calculated in this study (Figure 5). The νCO frequencies higher by 11−12 cm^{-1} in the Fe^{2+} state compared to the Fe^{3+} state (Table 1) suggest that the hydrogen bond with bicarbonate is stronger in the former state, in agreement with the prediction that the bicarbonate ligand is more negatively charged in the Fe^{2+} state. These considerations lead to a conclusion that the Tyr side chain coupled to the non-heme iron has a hydrogen bond donor−acceptor form in the Fe^{2+} and Fe^{3+} states, and one of the hydrogen bond partners is probably the bicarbonate ligand.

Structural Relationship of the Tyr with the Non-Heme Iron. The above discussion provides a view that only one Tyr side chain is strongly coupled to the non-heme iron. However, the X-ray structures of the PSII core complexes from *T. elongatus* reported by two independent groups (*5*, *7*) both reveal that two Tyr residues, D1-Y246 and D2-Y244, are located in the vicinity of the bicarbonate. These Tyr residues are symmetrically located, and no significant differences are found in the distances and orientations with respect to the bicarbonate (Figure 1and Table 3). The distances from the oxygen atom of D1-Y246 to O_A and O_C of bicarbonate are 3.2−4.0 and 3.0−3.6 Å, respectively, while those from the oxygen atom of D2-Y244 to O_A and O_B of bicarbonate are 3.6−4.5 and 3.2−3.3 Å, respectively. In addition, the $\angle CO\cdots O_{A,B,C}$ angles formed between the CO group of each Tyr and O_A, O_B, and O_C of bicarbonate are within 93−134°, while the $\angle O\cdots O_{B,C}C$ angles between the oxygen atom of each Tyr and the O_BC and O_CC groups of bicarbonate are 90−135°. In contrast, the $\angle O\cdots O_AC$ angles between the oxygen atom of each Tyr and the O_AC group of bicarbonate show smaller values of 53−94° that are not very appropriate for proper hydrogen bonding. Thus, both Tyr side chains have distances and orientations suitable for hydrogen bonding interactions with O_B or O_C of bicarbonate, indicating that they both can be a candidate for the Tyr strongly coupled to the non-heme iron detected by FTIR. It seems less likely, however, that the Tyr forms a strong hydrogen bond with O_A of bicarbonate.

Table 3: Distances and Orientations between D2-Y244 or D1-Y246 and the Bicarbonate or the Surrounding Amino Acid Residues Deduced from the X-ray Structures

	D1-Y246	D2-Y244
	Distances (Å)[a]	
$O\cdots O_A$[b]	4.0/3.2	3.6/4.5
$O\cdots O_B$[b]	—	3.3/3.2
$O\cdots O_C$[b]	3.0/3.6	—
O···N(K264)[c]	—	3.5/2.2
O···O(S268)[d]	4.1/4.2	—
	Angles (deg)[a]	
$\angle CO\cdots O_A$[b]	93/104	94/111
$\angle O\cdots O_AC$[b]	77/53	94/73
$\angle CO\cdots O_B$[b]	—	112/134
$\angle O\cdots O_BC$[b]	—	108/135
$\angle CO\cdots O_C$[b]	99/97	—
$\angle O\cdots O_CC$[b]	130/90	—
∠CO···N(K264)[c]	—	91/106
∠O···NC(K264)[c]	—	52/93
∠CO···O(S268)[d]	153/171	—
∠O···OC(S268)[d]	103/115	—

[a]The values were obtained from the X-ray structures at 2.9/3.5 Å [PDB entries 3bz1 (*7*)/1s5l (*5*)]. [b]O_A, O_B, and O_C are the oxygen atoms of the bicarbonate labeled in Figure 1. [c]N(K264) is the nitrogen atom of the D2-K264 side chain. [d]O(S268) is the oxygen atom of the D1-S268 side chain.

The X-ray structures also show that D1-S268 and D2-K264 are located within hydrogen bonding distance of D1-Y246 and D2-Y244, respectively (Figure 1 and Table 3), and thus can be candidates for another hydrogen bond partner of Tyr. Water molecules, which have not been resolved yet in the X-ray structures, also can form hydrogen bonds to the Tyr. Therefore, the most plausible view is that either D1-Y246 or D2-Y244 is coupled to the non-heme iron by providing a strong hydrogen bond to O_C or O_B of the bicarbonate ligand and simultaneously accepts a hydrogen bond from D1-S268, D2-K264, O_A of bicarbonate, or water to form a hydrogen bond network around the bicarbonate. The other Tyr may not directly interact with the bicarbonate and hence is rather insensitive to the redox change of the iron center. The coupling of D1-Y246 to the non-heme iron is consistent with the previous mutagenesis study in which the D1-Y246F mutant of *Synechocystis* sp. PCC6803 showed photoautotrophic growth slower than that of the wild-type cells (*43*), although it is also possible that this is due to the secondary effect caused by changing the hydrogen bond network around the iron center. Further mutagenesis studies in combination with FTIR analysis are necessary to definitively identify which Tyr residue is responsible for the strong coupling with the non-heme iron.

The coupling of a Tyr side chain to the bicarbonate is consistent with the previous observation by Berthomieu and Hienerwadel (*14*) that substitution of bicarbonate with other carboxylate anions induced the complete disappearance of the 1257 cm^{-1} peak, which is now definitively assigned to a Tyr signal. This disappearance may be caused by the loss of the direct interaction of the bicarbonate with D1-Y246 or D2-Y244 by

altered coordination structures of these carboxylate anions (*14*). Hienerwadel et al. (*28*) previously proposed that the bicarbonate has bidentate and unidentate coordinations in the Fe^{2+} and Fe^{3+} states, respectively. It is likely that the change of the Tyr νCO band upon the redox reaction of the iron center is coupled with this coordination change of bicarbonate. If the bicarbonate takes a unidentate ligand to Fe^{3+}, it should have an asymmetric structure with noncoordinating COH and CO groups. Thus, the idea that both D1-Y246 and D2-Y244 have identical hydrogen bond interactions in both Fe^{2+} and Fe^{3+} states providing very close νCO frequencies is rather unlikely.

Role of the Tyr Coupled with the Non-Heme Iron. The redox reaction of the non-heme iron is coupled to proton transfer (*13*−*15*), and the proton pathway around the non-heme iron involving bicarbonate may be directly relevant to the proton pathway to Q_B (*4*, *12*, *14*, *17*, *21*). This proton pathway may be formed by a rigid hydrogen bond network around the non-heme iron. Since the Tyr residue coupled to the iron center has a protonated form in both the Fe^{2+} and Fe^{3+} states (see above), it is not a titratable group responsible for the pH dependence (−60 mV/pH) of the E_m of the Fe^{3+}/Fe^{2+} couple (*10*, *11*). The Tyr residue may play a role in stabilizing the bicarbonate ligand by a strong hydrogen bond interaction. The fact that the Tyr OH group simultaneously forms two hydrogen bonds as a hydrogen bond donor and as an acceptor is essential in the formation of a rigid hydrogen bond network and a proton transfer pathway. Thus, it is proposed that the Tyr residue coupled to the non-heme iron has a key role in controlling the bicarbonate-relevant regulation of the quinone electron transfer and Q_B protonation reactions.

REFERENCES

1. Renger, G., and Holzwarth, A. R. (2005) Primary electron transfer. In Photosystem II: The Light-Driven Water:Plastoquinone Oxidoreductase (Wydrzynski, T., and Satoh, K., Eds.) pp 139−175, Springer, Dordrecht, The Netherlands.
2. Petrouleas, V., and Crofts, A. R. (2005) The quinone iron acceptor complex. In Photosystem II: The Light-Driven Water:Plastoquinone Oxidoreductase (Wydrzynski, T., and Satoh, K., Eds.) pp 177−206, Springer, Dordrecht, The Netherlands.
3. Diner, B. A., and Petrouleas, V. (1987) Q_{400}, the non-heme iron of the Photosystem II iron-quinone complex. A spectroscopic probe of quinone and inhibitor binding to the reaction center. *Biochim. Biophys. Acta 895*, 107–125.
4. Diner, B. A., Petrouleas, V., and Wendoloski, J. J. (1991) The iron-quinone electron-acceptor complex of photosystem II. *Physiol. Plant. 81*, 423–436.
5. Ferreira, K. N., Iverson, T. M., Maghlaoui, K., Barber, J., and Iwata, S. (2004) Architecture of the photosynthetic oxygen-evolving center. *Science 303*, 1831–1838.
6. Loll, B., Kern, J., Saenger, W., Zouni, A., and Biesiadka, J. (2005) Towards complete cofactor arrangement in the 3.0 Å resolution structure of photosystem II. *Nature 438*, 1040–1044.
7. Guskov, A., Kern, J., Gabdulkhakov, A., Broser, M., Zouni, A., and Saenger, W. (2009) Cyanobacterial photosystem II at 2.9-Å resolution and the role of quinones, lipids, channels and chloride. *Nat. Struct. Mol. Biol. 16*, 334–342.
8. Michel, H., and Deisenhofer, J. (1988) Relevance of the photosynthetic reaction center from purple bacteria to the structure of photosystem II. *Biochemistry 27*, 1–7.
9. Ikegami, I., and Katoh, S. (1973) Studies on chlorophyll fluorescence in chloroplasts II. Effect of ferricyanide on the induction of fluorescence in the presence of 3-(3,4-dichlorophenyl)-1,1-dimethylurea. *Plant Cell Physiol. 14*, 829–836.
10. Petrouleas, V., and Diner, B. A. (1986) Identification of Q_{400}, a high potential electron acceptor of Photosystem II, with the iron of the quinone-iron acceptor complex. *Biochim. Biophys. Acta 849*, 264–275.
11. Bowes, J. M., Crofts, A. R., and Itoh, S. (1979) A high potential acceptor for photosystem II. *Biochim. Biophys. Acta 547*, 320–335.
12. McEvoy, J. P., and Brudvig, G. W. (2008) Redox reactions of the non-heme iron in photosystem II: An EPR spectroscopic study. *Biochemistry 47*, 13394–13403.
13. Renger, G., Wacker, U., and Völker, M. (1987) Studies on the protolytic reactions coupled with water cleavage in photosystem II membrane fragments from spinach. *Photosynth. Res. 13*, 167–184.
14. Berthomieu, C., and Hienerwadel, R. (2001) Iron coordination in photosystem II: Interaction between bicarbonate and the Q_B pocket studied by Fourier transform infrared spectroscopy. *Biochemistry 40*, 4044–4052.
15. Mamedov, M. D., Tyunyatkina, A. A., Siletsky, S. A., and Semenov, A. Y. (2006) Voltage changes involving photosystem II quinone-iron complex turnover. *Eur. Biophys. J. 35*, 647–654.
16. Ishikita, H., and Knapp, E. W. (2005) Oxidation of the non-heme iron complex in photosystem II. *Biochemistry 44*, 14772–14783.
17. Van Rensen, J. J. S., Xu, C., and Govindjee (1999) Role of bicarbonate in the photosystem II, the water-plastoquinone oxido-reductase of plant photosynthesis. *Physiol. Plant. 105*, 585–592.
18. Van Rensen, J. J. S. (2002) Role of bicarbonate at the acceptor side of Photosystem II. *Photosynth. Res. 73*, 185–192.
19. Van Rensen, J. J. S., and Klimov, V. V. (2005) Bicarbonate interactions. In Photosystem II: The Light-Driven Water:Plastoquinone Oxidoreductase (Wydrzynski, T., and Satoh, K., Eds.) pp 329−345, Springer, Dordrecht, The Netherlands.
20. Eaton-Rye, J. J., and Govindjee (1988) Electron transfer through the quinone acceptor complex of photosystem II in bicarbonate-depleted spinach thylakoid membranes as a function of actinic flash number and frequency. *Biochim. Biophys. Acta 935*, 237–247.
21. Van Rensen, J. J. S., Tonk, W. J. M., and De Bruijn, S. M. (1988) Involvement of bicarbonate in the protonation of the secondary quinone electron acceptor of photosystem II via the non-haem iron of the quinone-iron acceptor complex. *FEBS Lett. 226*, 347–351.
22. Deligiannakis, Y., Petrouleas, V., and Diner, B. A. (1994) Binding of carboxylate anions at the non-heme Fe(II) of PS II. I. Effects on the $Q_A^-Fe^{2+}$ and Q_AFe^{3+} EPR spectra and the redox properties of the iron. *Biochim. Biophys. Acta 1188*, 260–270.
23. Noguchi, T., and Berthomieu, C. (2005) Molecular analysis by vibrational spectroscopy. In Photosystem II: The Light-Driven Water:Plastoquinone Oxidoreductase (Wydrzynski, T., and Satoh, K., Eds.) pp 367−387, Springer, Dordrecht, The Netherlands.
24. Berthomieu, C., and Hienerwadel, R. (2005) Vibrational spectroscopy to study the properties of redox-active tyrosines in photosystem II and other proteins. *Biochim. Biophys. Acta 1707*, 51–66.
25. Noguchi, T. (2007) Light-induced FTIR difference spectroscopy as a powerful tool toward understanding the molecular mechanism of photosynthetic oxygen evolution. *Photosynth. Res. 91*, 59–69.
26. Noguchi, T. (2008) Fourier transform infrared analysis of the photosynthetic oxygen-evolving center. *Coord. Chem. Rev. 252*, 336–346.
27. Debus, R. J. (2008) Protein ligation of the photosynthetic oxygen-evolving center. *Coord. Chem. Rev. 252*, 244–258.
28. Hienerwadel, R., and Berthomieu, C. (1995) Bicarbonate binding to the non-heme iron of photosystem II investigated by FTIR difference spectroscopy and ^{13}C-labeled bicarbonate. *Biochemistry 34*, 16288–16297.
29. Noguchi, T., and Inoue, Y. (1995) Identification of FTIR signals from the non-heme iron in photosystem II. *J. Biochem. 118*, 9–12.
30. Aoyama, C., Suzuki, H., Sugiura, M., and Noguchi, T. (2008) Flash-induced FTIR difference spectroscopy shows no evidence for structural coupling of bicarbonate to the oxygen-evolving Mn cluster in photosystem II. *Biochemistry 47*, 2760–2765.
31. Hienerwadel, R., Boussac, A., Breton, J., Diner, B. A., and Berthomieu, C. (1997) Fourier transform infrared difference spectroscopy of photosystem II tyrosine D using site-directed mutagenesis and specific isotope labeling. *Biochemistry 36*, 14712–14723.
32. Hienerwadel, R., Diner, B. A., and Berthomieu, C. (2008) Molecular origin of the pH dependence of tyrosine D oxidation kinetics and radical stability in photosystem II. *Biochim. Biophys. Acta 1777*, 525–531.
33. Noguchi, T., Inoue, Y., and Tang, X.-S. (1997) Structural coupling between the oxygen-evolving Mn cluster and a tyrosine residue in photosystem II as revealed by Fourier transform infrared spectroscopy. *Biochemistry 36*, 14705–14711.
34. Takahashi, R., Okajima, K., Suzuki, H., Nakamura, H., Ikeuchi, M., and Noguchi, T. (2007) FTIR study on the hydrogen-bond structure of a key tyrosine residue in the flavin-binding blue light sensor TePixD from *Thermosynechococcus elongatus*. *Biochemistry 46*, 6459–6467.
35. Sugiura, M., and Inoue, Y. (1999) Highly purified thermo-stable oxygen-evolving photosystem II core complex from the thermophilic

cyanobacterium *Synechococcus elongatus* having His-tagged CP43. *Plant Cell Physiol. 40*, 1219–1231.
36. Boussac, A., Verbavatz, J. M., and Sugiura, M. (2008) Isotopic labelling of photosystem II in *Thermosynechococcus elongatus*. *Photosynth. Res. 98*, 285–292.
37. Suzuki, H., Taguchi, Y., Sugiura, M., Boussac, A., and Noguchi, T. (2006) Structural perturbation of the carboxylate ligands to the manganese cluster upon Ca^{2+}/Sr^{2+} exchange in the S-state cycle of photosynthetic oxygen evolution as studied by flash-induced FTIR difference spectroscopy. *Biochemistry 45*, 13454–13464.
38. Frisch, M. J., Trucks, G. W., Schlegel, H. B., Scuseria, G. E., Robb, M. A., Cheeseman, J. R., Montgomery, J. A., Jr., Vreven, T., Kudin, K. N., Burant, J. C., Millam, J. M., Iyengar, S. S., Tomasi, J., Barone, V., Mennucci, B., Cossi, M., Scalmani, G., Rega, N., Petersson, G. A., Nakatsuji, H., Hada, M., Ehara, M., Toyota, K., Fukuda, R., Hasegawa, J., Ishida, M., Nakajima, T., Honda, Y., Kitao, O., Nakai, H., Klene, M., Li, X., Knox, J. E., Hratchian, H. P., Cross, J. B., Bakken, V., Adamo, C., Jaramillo, J., Gomperts, R., Stratmann, R. E., Yazyev, O., Austin, A. J., Cammi, R., Pomelli, C., Ochterski, J. W., Ayala, P. Y., Morokuma, K., Voth, G. A., Salvador, P., Dannenberg, J. J., Zakrzewski, V. G., Dapprich, S., Daniels, A. D., Strain, M. C., Farkas, O., Malick, D. K., Rabuck, A. D., Raghavachari, K., Foresman, J. B., Ortiz, J. V., Cui, Q., Baboul, A. G., Clifford, S., Cioslowski, J., Stefanov, B. B., Liu, G., Liashenko, A., Piskorz, P., Komaromi, I., Martin, R. L., Fox, D. J., Keith, T., Al-Laham, M. A., Peng, C. Y., Nanayakkara, A., Challacombe, M., Gill, P. M. W., Johnson, B., Chen, W., Wong, M. W., Gonzalez, C., and Pople, J. A. (2004) Gaussian 03 , revision C.02, Gaussian, Inc., Wallingford, CT.
39. Becke, A. D. (1993) Density-functional thermochemistry. III. The role of exact exchange. *J. Chem. Phys. 98*, 5648–5652.
40. Lee, C., Yang, W., and Parr, R. G. (1988) Development of the Colle-Salvetti correlation-energy formula into a functional of the electron density. *Phys. Rev. B 37*, 785–789.
41. Takahashi, R., and Noguchi, T. (2007) Criteria for determining the hydrogen-bond structures of a tyrosine side chain by Fourier transform infrared spectroscopy: Density functional theory analyses of model hydrogen-bonded complexes of *p*-cresol. *J. Phys. Chem. B 111*, 13833–13844.
42. Takeuchi, H., Watanabe, N., Satoh, Y., and Harada, I. (1989) Effects of hydrogen bonding on the tyrosine Raman bands in the 1300−1150 cm^{-1} region. *J. Raman Spectrosc. 20*, 233–237.
43. Kless, H., Oren-Shamir, M., Malkin, S., McIntosh, L., and Edelman, M. (1994) The D-E region of the D1 protein is involved in multiple quinone and herbicide interactions in photosystem II. *Biochemistry 33*, 10501–10507.